This manuscript was published as formal in:

Journal of Macromolecular Science, Part B. 2012 51(8) 1668-1680

DOI: 10.1080/00222348.2012.657134

https://doi.org/10.1080/00222348.2012.657134

***Title*:**

Structure-directed functional properties of symmetrical and unsymmetrical Br-substituted Schiff-bases

Luminita Marin [a], Valeria Harabagiu [a], Arie van der Lee [b], Adina Arvinte[c] and Mihail Barboiu*[a,b]

[a] *Petru Poni” Institute of Macromolecular Chemistry of Romanian Academy – 41A, Aleea Gr. Ghica Voda, Iasi, Romania*

[b] *Institut Européen des Membranes – ENSCM/UM2/CNRS 5635, IEM/UM2, CC 047, Place Eugène Bataillon, F-34095, Montpellier, France.*

[c]*Centre of Advanced Research in Nanobioconjugates and Biopolymers, “Petru Poni” Institute of Macromolecular Chemistry41A, Aleea Gr. Ghica Voda, Iasi, Romania*

Abstract

This study deals with the investigation of two low molecular weight Schiff base ompounds, differing only by the presence or absence of one methyl group, with the aim of better understanding the solution and the solid state optical and thermic properties generated by small structural features. The compounds were structurally characterized by ^{1}H-NMR, ^{13}C-NMR and FTIR spectroscopies, single-crystal X-ray diffraction and gas chromatography analysis. Their thermal behavior was evidenced by polarized light microscopy and differential scanning calorimetry. A comparison of the structures shows that the introduction of a Me unit as a bulky group hinders completely the π-π stacking interaction within the structural rows, inducing larger intermolecular distances resulting in rather different functional physical and chemical properties.

Keywords: Schiff base, bromine electronic effect, methyl substituent

1. Introduction

Schiff-bases compounds containing one or more CH=N imine bonds are intensely studied due to their large spectrum of physico-chemical properties: ability to form various coordination complexes, high thermal stability, semiconducting, liquid crystal, optical, therapeutic properties. As a consequence of their well-organised structures, all these features make them useful as thermo resistant materials, pharmaceutical products, or organic substrates in electronic and opto-electronic devices [1-5]. The easily procesable imine bonds [6] provide a direct access to complex systems like double helices [7], grids [8], borromean rings [9], dynamic polymers [10], capsules [11], polygons [12] etc. The self-organization of constitutional systems [13] resulting from reversible connectivity (molecular level) [14] and self-assembly (supramolecular level) [15] of subcomponents under the pressure of internal and external structural factors, is also endowing dynamic features for this type of compounds. Moreover, Schiff bases can give rise to extended conjugated platforms with unique optical, electronic and thermic properties. Depending on their molecular structure and composition, they can exist in various crystalline phases and only slight structural modifications can induce interesting modulation of functional properties.

In this context, we present here two examples of Schiff-bases prepared under mild reactional conditions, containing two bromo-phenyl moieties connected via an imine bond, combined with the existence of a methyl substituent in one compound rendering

unsymmetrical and influencing the planarity of the resulted bis-aromatic conjugated scaffold. It results quite different solid state optical and thermic properties generated by such small structural differences. The Br atom is almost inert from an electronic point of view due to two antagonistic electronic effects: a donor electronic effect due to the lone pair donor 4p orbital and a withdrawing effect due to a vacant 4d orbital acting as a weak electron acceptor [16]. Moreover, the Br moieties can be easily used as anchoring sites for further Suzuki coupling reactions [17, 18].

2. Experimental Section

2.1. Materials and methods: 4-Bromoaniline (97 % purity), 4-bromobenzaldehyde (99% purity), 4-bromo-3-methylaniline (99 % purity) purchased from Aldrich were used as received. The gas chromatograms were performed using an Agilent Network GC System 6890N instrument.

The infrared (IR) spectra were recorded on a FT-IR Bruker Vertex 70 Spectro-photometer in the transmission mode, by using KBr pellets.

The proton nuclear magnetic resonance (^{1}H-NMR) and carbon nuclear magnetic resonance (^{13}C-NMR) spectra were recorded by a BRUKER Avance DRX 400 MHz spectrometer using $CDCl_3$ as solvent and tetramethylsilane (TMS) as internal reference. Chemical shifts are reported in parts per million (ppm).

The elemental analysis was realised on an elemental analyzer CHNS 2400 II Perkin Elmer.

The UV–vis absorption and photoluminescence spectra were recorded on a Carl Zeiss Jena SPECORD M42 spectro-photometer and Perkin Elmer LS 55 spectrophotometer respectively, in very diluted DMF solutions ($\cong 10^{-5}$ %) using 10 mm quartz cells fitted with poly(tetrafluoroethylene) stoppers.

The thermal analysis was performed by using an Olympus BH-2 polarized light microscope equipped with a THMS 600/HSF9I heating stage. The optical observations were performed by using clean untreated glass slides. The differential scanning calorimetry (DSC) measurements were performed with a METTLER Toledo STAR system, under nitrogen atmosphere (nitrogen flow 120 ml/min, sample mass 3 – 4 mg). The transition temperatures were read at the top of the endothermic and exothermic peaks.

Wide angle X-ray diffraction measurements (WAXD) were performed on a Bruker D8 Advance diffractometer, using Ni-filtered Cu-Kα radiation (λ = 0.1541 nm). A MRI-WRTC – temperature chamber (with nitrogen inert atmosphere) and a MRI-TCPU1 – temperature Control and Power Unit were used. The working conditions were 36 kV and 30 mA. The

measuring angular range was 1.5-60° in 2θ. The samples for X-ray measurements were powders obtained by grinding single crystals formed by recrystallization from ethanol. All diffractograms are reported as observed. The single crystal diffraction intensities were collected at the joint X-ray Scattering Service of the Pôle Balard of the University of Montpellier II, France, at 175 K using an Agilent Technologies and a Gemini-S diffractometer with Mo-*K*α radiation. The structures were solved by *ab-initio* (charge-flipping) methods using *SUPERFLIP* [19] and refined by least-squares methods on *F* using *CRYSTALS* [20] against |*F*| on data having $I>2\sigma(I)$; *R*-factors are based on these data. Hydrogen atoms were located from difference Fourier synthesis, except the hydrogen atom in the CH=N linkage of compound **1** which was placed geometrically. Non-hydrogen atoms were refined anisotropically.

Cyclic voltammetry (CV) was employed to study the electrochemical behavior of **1** and **4** compounds deposited as thin films from $CHCl_3$ solution on the glassy carbon (GC) electrode. The cyclic voltametry (CV) measurements were performed using AUTOLAB PGSTAT302N system from ECO CHEMIE Utrecht, The Netherlands. The electrochemical studies were carried out in a single compartment electrochemical cell of 3 mL 0.1M tetrabutylammonium fluoride/acetonitrile, at room temperature under nitrogen atmosphere, using glassy carbon electrodes purchased from BASi – Bioanalytical Systems, Inc., USA as working electrode, an Ag/AgCl electrode and a platinum wire as reference and auxiliary electrodes. All reported potentials have been read *versus* Ag/AgCl.

2.2. Synthetic procedure for imine-compounds 1, 4

The synthesis of the (4-bromobenzylidene)-(4-bromo-phenyl)-imine (**1)** has been performed by the acid catalyzed condensation reaction of the 4-bromobenzaldehyde (**2)** with 4-bromoaniline (**3)** (Scheme 1).

5 mmol (0.88 g) of **3** and 4 ml ethanol were placed into a round bottom flask fitted with a condenser, a dropwise funnel, a nitrogen inlet and outlet. A solution of 5 mmol (0.93 g) of **2** in 4 ml ethanol was added slowly, under vigorous stirring, as well as few drops of glacial acetic acid as catalyst. The obtained mixture was gently refluxed overnight. The reaction mixture was kept for 24 hours until the crystals grew sufficiently. The crystals of **1** were filtered off, washed and recrystallized from ethanol. Finally, the obtained single crystals were dried under vacuum for 24 h. The yield was 87 %. The same experimental protocol has been applied for the synthesis of (4-Bromo-3-methyl-benzylidene)-(4-bromo-phenyl)-imine **4** from 5 mmol (0.94 g) of 4-bromo-3-methylaniline (**5)** and 5 mmol (0.93 g) of 4-

bromobenzaldehyde (**2**). The compound **4** resulted as white single crystals in 83 % yield. The gas chromatography confirmed the purity of the synthesised compounds to be more than 97% (Table 1S).

(4-bromobenzylidene)-(4-bromo-phenyl)-imine (**1**)

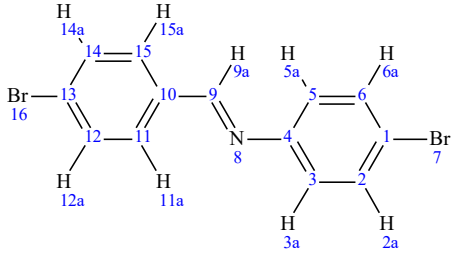

^{1}H NMR ($CDCl_3$, 400 MHz) : δ (ppm) 8.36 (s, 1H: C<u>H</u>=N); 7.76, 7.74 (d, 2H: 11a, 15a); 7.61, 7.59 (d, 2H: 12a, 14a); 7.51, 7.49 (d, 2H: 2a, 6a); 7.09, 7.06 (d, 2H: 3a, 5a). ^{13}C NMR ($CDCl_3$, 100 MHz): δ (ppm) 159.23(C9-H), 150.54(C4-ipso), 134.88 (C13-ipso), 132.24(C2-H; C6-H), 132.09(C12-H, C14-H), 130.19 (C11-H, C15-H), 126.19(C10-ipso), 122.54(C3-H, C5-H), 119.6(C1-ipso). FTIR ν: cm^{-1} (KBr): 814, 829, 1587 – 1478, 1620, 1723, 1895, 3062-2880. Calcd. for $C_{13}H_9Br_2N$ (339.03): C 46.06, H 2.68, Br 47.14, N 4.13; found: C 45.93, H 2.74, N 4.21.

(4-Bromo-3-methyl-benzylidene)-(4-bromo-phenyl)-imine (**4**)

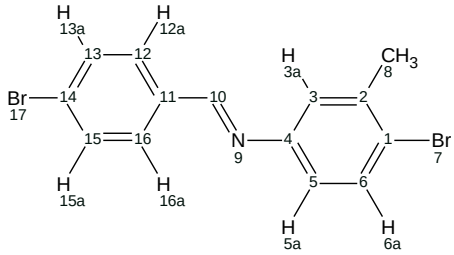

^{1}H NMR ($CDCl_3$, 400 MHz) : δ (ppm) 8.38 (s, 1H: C<u>H</u>=N); 7.77, 7.75 (d, 2H: 12a, 16a); 7.62, 7.60 (d, 2H: 13a, 15a); 7.54, 7.52 (d, 1H: 6a); 7.09 (s, 1H: 3a); 6.92, 6.90 (d, 1H: 5a); 2.43 (s, 3H: C<u>H</u>$_3$). ^{13}C NMR ($CDCl_3$, 100 MHz): δ (ppm) 159.07 (C10-H), 150.76 (C4-ipso), 138.78 (C2-ipso), 132.92 (C6-H), 132.09 (C13-H; C15-H), 130.17 (C12-H, C16-H), 126.19 (C14-ipso), 123.32 (C3-H), 122.15 (C1-ipso), 119.6 (C5-H), 22.9 (C8-H). FTIR ν: cm^{-1} (KBr): 818, 845, 1297, 1582 – 1461, 1618), 2852, 2921, 3077-2852. Calcd. for $C_{14}H_{11}Br_2N$ (353.06): C 47.63, H 3.14, Br 45.26, N 3.97; found: C 47.75, H 3.21, N 4.09.

3. Results and Discussion

3.1. Synthesis and structural characterization

The compounds **1** and **4** have been synthesized by classical acid condensation reaction (Scheme 1) [5, 21]. Single crystals have been obtained by recrystallization from ethanol. The ^{1}H, ^{13}C NMR and FTIR spectra are in agreement with the proposed formula (Figures 1, 2S). No significant differences have been observed, in the chemical shifts of either the N=C<u>H</u> proton or the aromatic protons, between the two synthetized azomethines, which indicates the weak influence of the inductive repulsive effect of the methylene unit. Despite the traces of reagents indicated by the GC measurements, no signals of initial compounds have been detected by NMR.

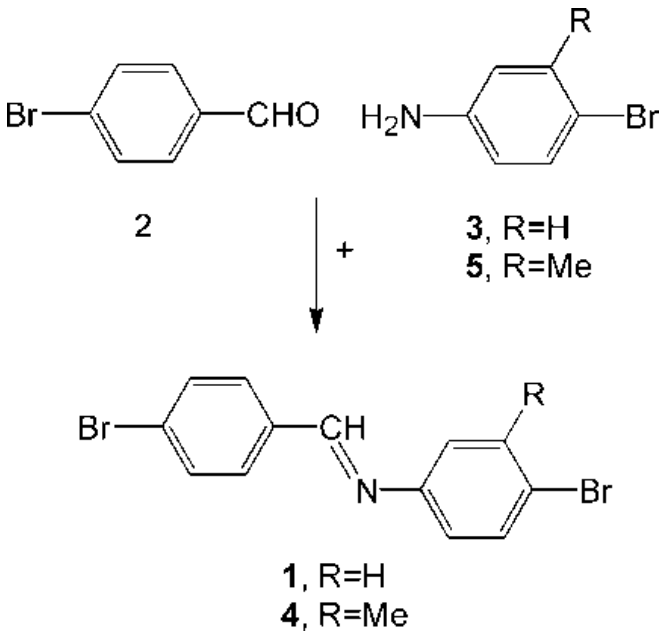

Scheme 1 Synthesis of compounds 1 and 4

The FTIR spectra show typical bands arising from imine groups presenting a strong absorption band at 1620 cm^{-1} and at 2880 cm^{-1} specific to the the –C=N- vibration and axial stretching of the C-H bond in the -CH=N- group, respectively (Figure 3S) [22]. No significant absorption bands were observed at 1685 cm^{-1} (due to the aldehyde group) or at 3345 cm^{-1} (due to the amine linkage). The weak absorption peaks at 3077–2991 and 1916–1723 cm^{-1} were assigned to the C-H stretching (ν_{C-H}) and the C-H out-of-plane (γ_{C-H}) deformations of the phenylene rings, respectively, while the strong absorption peaks within the 1587–1461 cm^{-1} and 845–708 cm^{-1} domains were attributed to the $\nu_{C=C}$ and γ_{C-H} of the 1,4-phenylene rings. Upon comparing the two spectra, as expected, the asymmetric and symmetric stretching modes of CH_3 in the **4** are assigned to the absorption bands at 2921 and 2852 cm^{-1} respectively, while the band at 1297 cm^{-1} is assigned to the C-CH_3 stretching mode. These findings are in very good agreement with the proposed structure and literature

values [23,24]. The FTIR spectra registered in the melted state reveals much more intense absorption bands than in the solid state, reflecting the disruption of intermolecular forces and thus increasing freedom of movement. In the case of compound **1**, the wave number of the absorption bands slightly move to blue, indicating that thermal energy favours the conjugation of the aromatic system, the linkages being weaker and their vibrations and deformations stronger. Contrary, the absorption bands of the compound **4** slightly moves to red, probably due to the hyperconjugation effect of the CH_3 unit which opposites to the withdrawing effect of imine nitrogen and increase the stability of the system (Figure 4S). The FTIR spectra, registered at room temperature, after cooling, are similar to the FTIR spectra before heating.

3.2. Solid state structures of imino compounds 1, 4

The crystal structures of **1** and **4** were determined on crystals obtained from ethanol solutions at room temperature. They reveal the expected azomethine compounds and the unit cells contain ten molecules of **1** and eight molecules of **4**, respectively. The molecule of **1** present a planar structure indicating a very good conjugation of imine linkage with phenyl moieties (the twisting angles of aromatic rings are both of 2.02°). In the crystal each molecule of **1** presents a tight contact with the two neighbouring ones by stacking with opposite orientations of the inner imine group side-arms (Figure 1). The occupancy of both imine atoms is corresponding to 50 % N and 50 % C while the C–H - atom is 50 % present in the two positions (Figure 1c). Each duplex of **1** associates in the crystal lattice by phenyl–phenyl offset–face–to–face (*off*) interactions (the average distance of 3.97 Å and the offset angle of about 20.8°) [25]. They are restricted to one direction forming interdigitated parallel rows which are alternatively stratified in compact stacked blocks (Figure 1b).

Figure 1. Crystal structure of compound **1**: a) side view in stick representation; b) space-filling representation of interdigitated parallel rows which are alternatively stratified in compact stacked blocks; c) side view of stacking offset-face-to-face interactions between two molecules of **1** in the crystal

Figure 2. Crystal structure of compound **4** in stick representation along a) *a*, b) *b*, and c) *c* axes

Within a row the distance between two Br–Br atoms of two different stacked ligands is 3.97 Å, indicating a slight cohesive interaction between the halogen atoms, the Van der Waals radius of Br being 1.85 Å, which enhances slightly the stabilization of the structure. This fact sustains the hypothesis of a push-pull system in which the two bromine atoms play antagonic role – withdrawing and repulsive, respectively – the sense being established by the nitrogen atom electronegativity. This is possible due to the two antagonistic electronic effect of bromine atom – the donor electronic effect due to the lone pair donor 4p orbital and the withdrawing effect due to a vacant 4d orbital – which become in a diffrent way predominant, forced by the nitrogen electronegativity. In the crystal two different blocks are arranged into almost two orthogonal planes (Figure 1a) with the inter-ribbons distance around 3.7 Å, forming molecular layers with the inter-layers distance about 12.4 Å, resulting in a fish backbone supramolecular architecture (Figure 1). The layers are weakly connected by type-II Br–Br interactions (3.801 Å; Θ_1=92.80°; Θ_2=166.00°), to be compared with the *cis*-type I Br–Br intralayer interaction (3.971 Å; Θ_1=71.36°; Θ_2=108.64°.[26] The inter-molecular and inter-ribbons distances are close to the interplanar π-π distance of 3.5 Å, pointing for presumed electrical properties.

The molecule of **4** presents a non-planar distorted geometry with the torsion angles C-C-C=N and C=N-C-C of -15.07 and 20.6º, respectively, indicating a very low conjugation of imine linkage with phenyl moieties. The molecules of **4** are in close contact filling the space of the crystal, but in contrast to compound **1** no π–π stacking interactions are present within the crystal. The integrity of the crystal packing is assured by weak hydrophobic CH_3–CH_3 and interlayer halogen Br–Br (d=3.881 Å) contacts. The latter contacts have a trans type I configuration with Θ_1=112.5° and Θ_2=152.9°. In addition to these interlayer contacts, there is an attractive CH…Br contact of 2.95 Å with a CH…Br angle of 141.7°. The molecules are forming ribbons along *b* axis with an intermolecular distance of 6.13Å, the packing being driven by self assembling of aromatic rings and methyl groups. The ribbons are packed together two by two, with an inter-ribbons distance of 3.79 Å, while the d-spacing between the twice packs is 4.10 Å. The packs form molecular layers, with the inter-layer distance about 14.7 Å.

Figure 3 show the packing interactions in the structures of **1** and **4**, as calculated from the gradient of the electron densities derived from the atomic coordinates [27,28]. It is clearly shown that the packing of the molecules within the layers in **1** is mostly driven by π–π stacking interactions between the molecules within the rows which are in close contact via

van der Waals interactions so that all available void space between the molecules is filled. Oppositely, only weak van der Waals interactions may be observed in the structure of the compound **4**, presenting a less dense structure than compound **1**.

Figure 3. Packing interaction areas (translucent red surfaces) in the single crystal structures of compounds a) **1** and b) **4**

The X-ray crystallographic results allow the following conclusions to be made:

- In term of specific self-assembly the compounds **1** and **4** self-organize in the solid state in interdigitated parallel rows which are alternatively stratified in compact stacked blocks.
- The larger intermolecular distances observed between rows and blocks in the crystal matrix, indicate that compound **4** presents a lower dipole moment than compound **1** because of the Me electron-donor bulky group on the aniline ring which favors an increase of the dihedral angle and strongly disturb the planar interactions between molecules.
- The bromine substituents have a dynamic electronic effect drawn by the structural environment.
- In term of specific self-organization the compounds **1** and **4** reveal an attractive example of solid-state high (**1**) or low (**4**) density structures resulted by synergetic intermolecular π-π stacking, halogen-halogen, halogen-H, and hydrophobic CH_3- CH_3 interactions between different molecules.

3.2. UV-vis and fluorescence spectra

The ultraviolet (UV-vis) absorption and fluorescence spectroscopic data in diluted dimethylformamide (DMF) solution ($5x10^{-4}$M) for the azomethine compounds **1** and **4** are summarized in Table 2. The absorption spectra are characte-rized by two absorbtion bands: the first one at 278 nm (4.46 eV) assigned to the benzenoid transitions and the second one at 325 and 322 nm, respectively (3.81, 3.85 eV) characteristic to the spin-allowed π-π* transitions involving the azomethine-phenyl-bromine framework (Figure 4).

Figure 4. Absorption and emission behaviour of **1** (continuous line) and **4** (dashed line)

The marked broadening of the absorption peaks can be related to different conformations adopted in the solution. The incorporation of the CH_3 group do not result in notable effects

on the position of λ_{max} band for the compounds **1** and **4**. The energy band gap (E_g) was estimated from the following equation: $E_g = h \times c / \lambda_{max}$, where h is the Planck constant, c is the light velocity, and λ is the wavelength of the absorption, in the optical absorption spectra. The energy band gap has been calculated for wavelength of the absorption maxima, edge absorption and for the intercept of absorption and emission spectra. This simple method allows for the estimation and then the comparison of the energy gaps of the investigated compounds in the form of solution, as it is gathered in Table 2. The values of the optical band gaps (E_g^{opt}) estimated from their absorption maxima are higher than those usually observed for azomethine compounds incorporating in their structure electron-withdrawing units which promote conjugation [3, 21].

The emission spectra of compounds **1** and **4** have been measured by excitation at 278 nm. They are luminescent materials which emit weak violet (414 nm) and bluish light (425 nm), respectively (Figure 4). Interestingly enough, the compounds present large Stokes shift values (89 and 103 respectively), resulting in an overlap missing between the absorption and emission spectra of the compound **4** and a negligible overlap in the case of **1**. This prevents the reasorbtion of the emitted light and so undesired loses, aspect very important for applications based on detection of emitted light or light emitting devices [5, 29].

3.3. Thermal structural behaviour

The polarized light microscopy (PLM) measurements showed that compounds **1** and **4** present well-defined crystalline states at room temperature, (Figure 5) which rapidly melt during the first heating scan with a short appeareance of marbled textures not reliable with stable mesophases observed for other systems [30, 31]. The melting point of the less compact structure of the **4** (81 ^oC) is substantially lower than the melting point of dense structure of **1** (147^oC) in accordance with observed crystal structure. When the isotropic liquid is cooled, the crystalline state appears in the form of terraces and spherules, respectively at 130^oC (**1**) and 43 ^oC (**4**).

The differential scanning calorimetry (DSC) measurements (Figure 5S) are consistent with PLM observations: melting with the short occurrence of the marbled texture (endothermic left tailed peak at 143 ^oC (**1**) and 81^oC (**4**)) and crystallization processes (exothermic peak at 135 ^oC (**1**) and 49 ^oC (**4**)). The melting and crystallization temperature values determined by DSC are close by those measured by PLM, under the same conditions (10^oC/min). The DSC and PLM measurements registered with various heating/cooling rates (10, 5, 1^oC) show only a

melting and, respectively, cooling process, indicating that, in the absence of a flexible spacer, the mesophase could not be stabilized.

Figure 5. Polarized light microscopy photographs (200x) of compounds 1 and 4 a) before and b) after heating/cooling cycle

The X-ray diffraction patterns of the compounds **1** and **4** have been recorded for the samples obtained by recrystallization from ethanol and then for the samples thermally treated (heating up to the melted state and cooling at room temperature) (Figure 6). It appears that already before the thermal treatment the samples are not single-phased, because not all peaks can be indexed using the cell parameters of the single-crystal structure determinations. Both **1** and **4** display a pronounced impurity peak at a slightly lower angle than the main (*002*) diffraction peak of the single-crystal crystalline phases. The (*002*) peak corresponds to the packing direction of the layers formed by the interdigitated parallel rows and which are hold together by very weak Br-Br interactions and in the case of compound 4, by a slightly stronger CH…Br interaction. These interactions are so weak that other interactions may be possible to self-assemble the 3D structure, which explains qualitatively the formation of a second polymorphic crystal form for both **1** and **4**. Based on the relative intensities of the strongest peaks of both forms, it is estimated that about 80% of the crystals are of the form determined by single-crystal diffractions, and that the remaining 20% belong to an unknown polymorph.

Upon thermal treatment the behaviour of **1** and **4** is different. The diffraction intensities in both cases diminish, but for **1** a new polymorph appears to develop at the expense of both room-temperature polymorphs, whereas no signs of a new polymorph appear for **4**. Peak broadening is insignificant upon the thermal treatment, meaning that the coherently diffracting domains do not become smaller. The drop in relative intensity of **4** is therefore a bit surprising, since the appearance of an important signal originating from an amorphous part cannot be detected as well.

Fig. 6 XPRD diffraction patterns of compounds **1** (left) and **4** (right) at room temperature. The top figures represent the diffractograms before thermal treatment along with the Le Bail fits using the cell parameters of the single crystal structure determinations. Blue lines are the observed diffraction patterns and red lines the calculated patterns. The arrows indicate some of the diffraction peaks belonging to the second phase. The bottom figures represent the

superimposed XPRD patterns before and after thermal treatment; the blue lines are the patterns before treatment and the red lines those after thermal treatment.

3.3. Electrochemical experiments

The electrochemical behavior of the compound **1** deposited as a film on the glassy carbon electrode was evaluated by cyclic voltammetry at a scan rate of 100 mV/s using 0.1M tetrabutylammonium fluoride in acetonitrile as supporting electrolyte. As shown in Figure 7, when scanning the potential on the negative range, only one reduction peak appears around -1.08 V attributed to the reduction of imino group. Applying the potential in the positive range, two oxidation peaks at +1.15V and +1.39 V were registered due to the electron transfer processes taking place at the terminal bromine. Compared to compound **1**, the reduction peak corresponding to compound **4** occurs at more negative potential value (-1.34 V) (Figure 7a) and with a lower current intensity, indicating a more difficult reduction process. The explanation for this negative shift might be the hyperconjugation effect due to the presence of the methyl group which diminishes the electron density of the molecules. On the other hand, the oxidation peaks of the compound **4** is left shifted to lower potential values (+1.07 V and +1.29 V) indicating an easier oxidation, facilitated by the electron-donor methyl group (Figure 7b).

To establish the electronic structure of **1** and **4** compounds, the relative energy levels of the highest occupied molecular orbital (HOMO or π level) and the lowest unoccupied molecular orbital (LUMO or π* level) have been estimated from cyclic voltammetric measurements on the basis that the oxidation process corresponds to electrons removal from HOMO energy level, while reduction corresponds to electron addition to the LUMO energy level of material.[32] The oxidation onset potentials (E_{onset}^{ox}) and reduction onset potentials (E_{onset}^{red}) of a material can be correlated to the ionization potential and electron affinity according to the relationship proposed by Bredas et al.[33] The onset potentials are obtained at the intersection of the baseline charging current with the tangent drawn at the rising currents. A summary of the peak potentials (E_{ox}, E_{red}), oxidation and reduction onset potentials of the two compound is given in Table 3. The ionization potentials (IP) and electron affinity (AE) have been calculated, according to equations:

$$IP = E_{onset}^{ox} + 4.4 \text{ (eV)}$$

$$AE = E_{onset}^{red} + 4.4 \text{ (eV)}$$

$$E_g = IP - AE \quad (eV)$$

where E_{ox} and E_{red} are the onset potentials of oxidation and reduction measured in the system, while E_g is the energy gap.

Figure 7. Comparison of voltammetric profiles in a) the reduction and b) the oxidation range for **1** (solid line) and **4** (dotted line)

As can be seen from Table 3, the HOMO level of the compound **1** is higher and its electrochemical band gap is smaller compared to the compound **4**, due to the better conjugation and thus better planarity of the molecules.

4. Conclusions

In conclusion the simple symmetrical and unsymmetrical Schiff bases discussed here present complete different constitutional, optical and thermic properties. The presence of a CH_3 bulky group on the aromatic backbone influences the electronic its properties by decreasing the HOMO energy level and the increasing of energy gap which hinder the electronic transitions. Moreover, the shifting of emission from violet to bluish leads to an overlap missing between absorption and emission spectra which prevent the reasorbtion of the emitted light. Comparing the crystal packing of the two compounds, the introduction of a Me unit as a bulky group in the chemical structure of **4**, hinders completely the weak π-π stacking interaction within the rows, inducing larger intermolecular distances which significantly differentiates the properties of compounds **1** and **4**. The crystalline structure obtained by crystallization from the melted state shows closer intermolecular distances when compared to the supramolecular architecture of the crystalline structure obtained by recrystallization from ethanol. More precisely, about 80% of the crystals are of the form determined by single-crystal diffraction, and the remaining 20% belongs to an unknown polymorph. Considering the simplicity of this molecules, these basic molecular synthons can further find possible applications on the synthesis of more complex heteroarchitectures of applicative interest.

Acknowledgements

The research leading to these results has received funding from the Romanian National Authority for Scientific Research, CNCS – UEFISCDI grant, project number PN-II-ID-PCCE-2011-2-0028 and European Union's Seventh Framework Programme (FP7/2007-2013) under grant agreement n°264115 - STREAM.

Electronic Supplementary Information (ESI) available: Suplementary NMR FTIR, DSC, gas chromatography, cif files and XPRD data. See DOI: 10.1039/b000000x/

[#]CCDC 924133 and 924134 contain the supplementary crystallographic data for this paper. These data can be obtained free of charge from The Cambridge Crystallographic Data Centre via www.ccdc.cam.ac.uk/data_request/cif.

1. A. Iwan, D. Sek, *Progr. Polym. Sci*., 2008, **33**, 289-345.
2. S. Kumar, D. N. Dhar, P. N. Saxena, *J. Sci. Ind. Res.*, 2009, **68**, 181-187.
3 D. Sek, A. Iwan, B. Jarzabek, B. Kaczmarczyk, J. Kasperczyk, Z. Mazurak, M. Domanski, K. Karon, M. Lapkowski, *Macromolecules*, 2008, **41**, 6653-6663.
4 S. Andres. P. Guarin, S. Dufresne, D. Tsang, A. Sylla, W. G. Skene, *J. Mater. Chem*., 2007, **17**, 2801–2811.
5 A. Zabulica, M. Balan, D. Belei, M. Sava, B. C. Simionescu, L. Marin, *Dyes and Pigments* 2013, **96**, 686-698.
6 M. Barboiu, F. Dumitru, Y.-M. Legrand, E. Petit, A. van der Lee, *Chem. Commun.*, 2009, 2192-2194
7 Y. M. Legrand, F. Dumitru, A. van der Lee, M. Barboiu, *Chem. Commun*, 2009, 2667-2669
8 M. Barboiu, M. Ruben, G. Blasen, N. Kyritsakas E. Chacko, M. Dutta, O. Radekovich, K. Lenton, D. J. R. Brook and J.-M. Lehn, *Eur. J. Inorg. Chem*., 2006**,** 784-789.
9 C. D. Pentecost, K. S. Chichak, A. J. Peters, G. W. V. Cave, S. J. Cantrill, J. F. Stoddart, *Angew. Chem., Int. Ed.*, 2007, **46**, 218–222.
10 L. Marin, B. Simionescu, M. Barboiu, ***Chem. Commun.***, 2012, **48**, 8778-8780.
11 C.G. Claessens, M.J. Vicente-Arana, T. Torres, *Chem. Commun.*, 2008, 6378–6380.
12 B.H. Northrop, H-B.Yang, P.J. Stang, *Inorg. Chem.*, 2008, **47**, 11257-11268.
13 a) J.-M. Lehn, *Chem. Soc. Rev.* 2007, **36**, 151-160; b) M. Barboiu, *Chem. Commun* 2010, **46**, 7466-7476 ; c) M. Barboiu, J.-M. Lehn, *Proc. Natl. Acad. Sci. USA*, 2002, **99**, 5201-5206.
14 a) F. Dumitru, E. Petit, A. van der Lee, M. Barboiu, *Eur. J. Inorg. Chem.*, 2005, 4255–4262; b) Y.M. Legrand, A. van der Lee, M. Barboiu, *Inorg. Chem.*, 2007, **46**, 9083-9089
15 a) M. Michau, M. Barboiu, R. Caraballo, C. Arnal-Hérault, P. Periat A. van der Lee, A. Pasc, *Chem. Eur. J.*, 2008, **14**, 1776-1783 b) C. Arnal-Hérault, M. Barboiu, A. Pasc, M. Michau, P. Perriat, A. van der Lee, *Chem. Eur. J.* 2007, **13**, 6792-6800; A. Cazacu, Y.M. Legrand,

A. Pasc, G. Nasr, A. van der Lee, E. Mahon, M. Barboiu, *Proc. Natl. Acad. Sci.*, 2009, **106**, 8117-8122;

16 Z. Havlas and J. Michl, *J. Am. Chem. Soc*., 2002, **124**, 5606-5607.

17 L. Marin, S. Destri, W. Porzio, F. Bertini, *Liq. Cryst*. 2009, **36**, 21-32.

18 M. Grigoras, N. C. Antonoaia, *Polymer Int.*, 2005, **54**, 1641-1646.

19 L. Palatinus, G. Chapuis. *J. Appl. Cryst.* 2007, **40**, 786-790.

20 P. W. Betteridge, J. R. Carruthers, R. I. Cooper, K. Prout, D.J. Watkin. *J. Appl. Cryst.*, 2003, **36**, 1487.

21 L. Marin, V. Cozan and M. Bruma. *Rev. Roum. Chim*., 2005, **50**, 649-653.

22 A. M. Machado, J. D. Da, Motta Neto, T. D. Z. Atvars, L. Akcelrud, *J. Luminescence*, 2009, **129**, 720-728.

23 G. Varsany, Vibrational Spectra of Benzene Derivatives, Academic Press, New York, 1962.

24 N. Sundaraganesan, H. Saleem, S. Mohan, M. Ramalingam and V. Sethuraman, *Spectrochim. Acta A* 2005, **62**, 740-751.

25 F. Dumitru, E. Petit, A. van der Lee, M. Barboiu, *Eur. J. Inorg. Chem.*, **2005**, 4255–4262.

26 N. Ramasubbu, R. Parthasarathy, P. Murray-Rust, *J. Am. Chem. Soc.* 1986, **108**, 4308-4314

27 E. R. Johnson, S. Keinan, P. Mori-Sánchez,, J. Contreras-García, J., A. J. Cohen, W. Yang,., *J. Am. Chem. Soc.*, 2010, **132**, 6498-6506.

28 J. Contreras-García, E. R. Johnson, S. Keinan, R. Chaudret, J. Piquemal, D. N. Beratan, W. Yang, *J. Chem. Theory Comput***,** 2011, **7** 625-632.

29 B. Behramand, F. Molin H.Gallardo, Dyes Pigments, 2012, **95**, 600-605.

30 J. A. Castellano, J. E. Goldmacher, L. A. Barton, J. S. Kane, *J. Org. Chem.*, 1968, **9**, 3501-3504.

31 S-T. Ha, T-L. Lee, S.-L. Lee, S. S. Sastry, Y-F. Win, *Sci. Res. Essays* 2011, **6**, 5025-5035.

32 S. Janietz, D.D.C. Bradley, M. Grell, M. Giebeler, M. Inbasekaran, E.P. Woo, *Appl. Phys. Lett.* 1998, **73**, 2453-2455.

J. L Bredas, R. Silbey, D.X. Boudreux, R.R. Chance, *J. Am. Chem*